Available online at www.sciencedirect.com
ScienceDirect
International Journal of Rock Mechanics & Mining Sciences 45 (2008) 564–573
International Journal of Rock Mechanics and Mining Sciences
www.elsevier.com/locate/ijrmms

Quantifying the evolution of static elastic properties as crystalline rock approaches failure

M.J. Heap*, D.R. Faulkner

Rock Deformation Laboratory, Department of Earth and Ocean Sciences, University of Liverpool, Liverpool L69 3BX, UK

Received 5 April 2007; received in revised form 3 July 2007; accepted 18 July 2007
Available online 4 September 2007

Abstract

The pervasive damage of rock by dilational microcracks strongly influences rock strength and macroscopic elastic properties. In this study, two types of experiment were performed to investigate and quantify the contribution of microcracking to the static elastic response of Westerly granite as it approaches failure. They are (1) increasing-amplitude cyclic loading experiments and (2) constant-amplitude cyclic loading experiments, some of which incorporated a 'load-hold' component to explore the elastic response of time-dependent effects such as stress corrosion. We report values for the tangent moduli in the region of the stress–strain curve where the values are the same for an unloading cycle as they are for the subsequent loading cycle. Hence, although there is hysteresis between these two curves, we assume perfect elasticity in this region. This approach allows the evolution of static elastic properties as rock approaches failure to be documented in great detail, in contrast to previous work that has generally been limited to the linear elastic region of the stress–strain curve. Increasing-amplitude stress cycling causes a gradual reduction in sample stiffness, equating to a decrease in Young's modulus (~11%) and an increase in Poisson's ratio (~43%) measured at a constant stress level. Elastic properties are also seen to have a strong stress-dependency during loading (~46% increase in Young's modulus from 20 to 100 MPa). Experiments devised to promote time-dependent microcracking had a negligible contribution to the evolution of static elastic properties over the timeframe and dry conditions under which our experiments were conducted. Such results can be applied to our understanding of the mechanics, stress distribution and fault displacement models within and surrounding fault zones.

Keywords: Static elastic properties; Microcracking; Stress cycling; Stress corrosion; Uniaxial compression

1. Introduction

Elasticity is a fundamental physical property of rock. It controls the distribution and magnitude of sub-yield stress within the Earth's crust, the propagation of elastic (seismic) waves through rocks and is used to relate strain measurements to in situ stresses present in the crust. Distributed damage and imperfections affect the rock strength and elastic properties and are ubiquitous in materials, including rocks under crustal stress conditions [1,2]. Stressing brittle rock leads to the further development of distributed damage [3], which is manifest as dilational microcracks and can eventually lead to brittle failure [4,5].

Research on the topic has generally been biased towards the effect of 'damage' on the ultimate failure strength (damage mechanics), and less attention has been directed towards the effect of microcracking on the elastic properties of rocks. However, the evolution of elastic properties as rock approaches failure has many important geological applications. Among these applications is the understanding of stress surrounding geological faults. Faults have been shown to have a high microcrack density near the fault core that decreases exponentially with distance [6–10]. Faulkner et al. [11] showed that these microcracks change the elastic properties of rock and hence the stress state surrounding faults. Hence a change in elasticity for rocks in fault zones has implications for the mechanics, stress distribution and fault displacement models within and

*Corresponding author. Now at Mineral, Ice and Rock Physics Laboratory, Department of Earth Sciences, University College London, Gower Street, London WC1E 6BT, UK.
E-mail address: m.heap@ucl.ac.uk (M.J. Heap).

1365-1609/$ - see front matter © 2007 Elsevier Ltd. All rights reserved.
doi:10.1016/j.ijrmms.2007.07.018

surrounding fault zones. These effects are not limited to fault zones, and increased microcrack density in any part of the brittle crust is likely to result in a change in the state of stress if the elastic properties are modified by crack density.

As an illustration of the problems encountered we provide the following examples. Both linear elastic and non-linear elastic (or post-yield) crack models predict a linear relationship between rupture displacement during an earthquake or total fault displacement (u) and either rupture length or total fault length (L); however, attempts to find universal-scaling laws for L/u have generally failed [12]. Some have suggested that these models have partly failed because they do not take into account the changes in mechanical properties, in particular Young's modulus as the fault zone evolves [13]. This was supported observations made by Peltzer et al. [14] where interferometric synthetic aperture radar observations of the 1997 Manyi earthquake in Tibet infer non-linear elastic behaviour of the crust that is dependent on the stress applied (compressive or tensile). Non-linear elastic crack models generally invoke some region of yield around the crack or rupture tip, and this is often interpreted as a cloud of microcracks [15]. Although in these computations the yield strength of the rock is specified and microcracking or yield is expected at approximately 50% of the yield stress [8], the accompanying changes in the elastic properties are not accounted for. Stresses and displacements around underground excavations are also often calculated assuming linear elasticity. This leads to erroneous predictions of the deformation and of the initiation and extent of failure around underground excavations [16]. Brown et al. [16] report that using a slightly modified theory that incorporates elastic moduli that change with confining pressure, results are more consistent with aspects of those obtained in hydrostatic compression tests. Lau and Chandler [17] have also highlighted the use of elastic properties in the design of deep geologic repositories. The characterization of elastic moduli evolution as rock approaches failure can provide further improvement to such calculations.

Several experimental studies have shown that elastic properties [17–21] depend on the extent of damage within a rock. Theoretical approaches to characterizing rock elastic properties have also been used. Lyakhovsky et al. [22] use models to predict changes in the effective elastic modulus against axial strain, focusing on the change as loading reverses from uniaxial compression to uniaxial tension. However one of the principal shortcomings of previous work has been that the elastic properties are only calculated in the linear elastic region and hence valuable information on the elastic properties at stresses closer to failure (in the non-linear elastic region) are not given [e.g. 18,21]. Typically the linear elastic region ranges only up to ~40% of the failure stress and consequently there is a great deal of information lost. In other work, the 'elastic properties' are quoted at stresses above the linear elastic region, but these values are simply the local gradient of the stress–strain curve (the 'tangent' moduli), or the ratio of the principal strains (for Poisson's ratio), without any attempt to establish if the non-linear portion of the stress strain curve is reproducible and hence elastic. Indeed, in many cases, the quoted values for 'Poisson's ratio' are in excess of 0.5, indicating inelasticity [17,19].

Time-dependent brittle deformation is a fundamental and ongoing process in the Earth's upper crust, and leads to the failure of rock at relatively low stresses. Static fatigue or 'brittle creep' tests used to study this process have generally only considered the long-term strength of crystalline rock [19,23–28], but have yet to explore its potential influence on the development of crack networks leading to changes in the elastic properties.

The change in elastic properties during deformation can also be monitored by inversion of the ultrasonic wave velocities measured in experiments, given the density and assuming isotropy [29–39]. However, it has long been recognized that there are differences in the static and dynamic elastic properties of rocks [40–44]. This is due to the amplitude and frequency of the stress that is applied to the rock, and grain scale response to these applied stresses—such as intrinsic inelasticity. As Ciccotti and Mulargia [43] note: 'the static response of rocks to large-scale stresses can be quite different from that estimated by the seismic measurements and should be investigated further'.

In light of all this previous work, we conclude that the characterization of static elastic property development for fractured rock approaching failure is a fundamental, yet poorly understood phenomenon. In this work we aim to measure elastic properties outside the linear elastic region and hence quantify elastic property development at stresses closer to sample failure. Our study quantifies the change in static elastic properties as a product of large amplitude stress cycles using a new methodology to determine the elastic properties in the non-linear elastic part of the stress strain curve. It allows the tangent elastic moduli to be determined for specific values of applied stress. We also perform 'load-hold' tests in order to try to identify any time-dependent processes that may be operative and their effect on the elastic properties. The paper first introduces background and previous work on rock elastic properties. We then explain experimental technique and how the data were interpreted to obtain static elastic properties. Finally, we present results from the tests and briefly discuss these results in light of the likely micromechanical processes that may be operative.

2. Experimental procedure

In this study, two types of experiment were performed to investigate the contribution of microcracking to the resultant strain damage and static elastic response of rock approaching failure. They are (1) increasing-amplitude cyclic loading experiments and (2) constant-amplitude cyclic loading experiments, some of which incorporated a 'load-hold' component. All experiments were performed on

oven-dried (at 80 °C, see [45]), 1 in diameter cylindrical samples of initially intact Westerly granite and conducted using an unconfined (σ_2 and $\sigma_3 = 0$), uniaxial compression apparatus. Westerly granite (from south-east Rhode Island, USA) has been extensively tested in rock mechanics due to its small grain size, low initial crack density and that it is generally considered to be isotropic [27,46 and references therein]. Hence it can yield a high level of experiment reproducibility under carefully controlled test conditions.

It is pertinent to note however that Hadley [47,48] and Scholz and Koczynski [49] described Westerly granite as exhibiting mild dilatancy anisotropy; also, granite is usually inherently anisotropic in its mechanical behaviour due to the existence of preferentially oriented microcracks [50,51, and references therein]. The experimentally induced microcracking will encourage an anisotropic fabric within the sample [34,52], resulting in anisotropic elastic property development as deformation progresses. In our study, as in many other previous experimental studies involving Westerly granite, we assume isotropy within the sample, and if the change in elastic parameters in directions other than the principal strain axes is required, then further, more elaborate experiments would be required.

The samples were cored from the same block, in the same direction (see Fig. 1 for core orientation) to allow results to be comparable even with the existence of a mild anisotropy fabric, cut so their length-to-diameter ratios were in excess of 2.5 [53] and precision-ground to strict tolerances (± 0.02 mm) as to the squareness of their edges. Steel spacers, of the same diameter as the specimen, were used at each end of the sample and held in place by plastic tubing to help reduce the problem of 'end effects' [53]

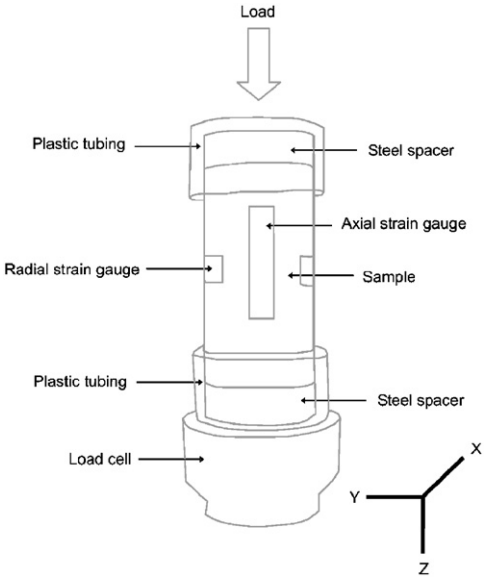

Fig. 1. Schematic diagram showing sample set-up during experimentation. Core orientation is also indicated for use in conjunction with thin section photomicrographs. *Z*-direction is along the sample axis.

(Fig. 1). All of the above factors are fundamental for the production of a viable data set [54].

Strain gauges in an axial and circumferential configuration were wired into a full Wheatstone bridge circuit, which utilized a dummy sample, and were used to monitor the development of the principal strains (Fig. 1). All strains, and stress from the load cell, were continuously recorded during experimentation. The stress was increased and decreased by small increments (~2 MPa) during experiments via a hand-controlled valve and the load-rate was kept at approximately 2.5 MPa/min. The unconfined compressive strength (UCS) of the cored Westerly granite samples was determined to be ~200 MPa (from samples WG-01 and WG-02). All experiments were carried out under ambient laboratory conditions, with temperatures ~20 °C. Test conditions for all experiments are summarized in Table 1.

Many researchers have investigated the stress–strain behaviour of brittle rock under compression. The failure process can be broken down into a number of stages (Fig. 2) characterized by changes in the axial and circumferential strain response recorded during uniaxial compression tests [19,21,55–57]. The stages include: OA, the region where the stress–strain response is concave upwards; AB, the region where the stress–strain behaviour is very nearly linear; BC, the region where the stress–strain response is concave downwards; and after C, post-peak behaviour, dependent on the stiffness of the testing machine, can be seen following the peak stress.

The elastic properties of materials are generally obtained from region AB of the curve, where the linear elastic constants can be determined. However, as long as there is a reproducible relationship between stress and strain such as for a perfectly elastic material, the relationship need not necessarily be linear. Perfect elasticity implies that, during loading and unloading, the same path is followed. Hence the energy stored in the specimen during loading will be released during unloading. In this case there are no unique values for the elastic moduli; instead there will be a range of values corresponding to the level of stress on the specimen. These elastic parameters can be obtained by the local gradient of the stress–strain curve (termed the 'tangent' modulus in [55]).

In the case of rocks, however, perfectly elastic behaviour does not strictly occur, as once the yield point is exceeded there is hysteresis, implying that some of the energy stored during loading has been dissipated into the specimen. In low temperature experiments, this energy is generally assumed to be used to create new crack surface area. In order that we might obtain elastic parameters in the non-linear region of the stress strain curve, a test for perfect elasticity, or something approximating to it, is required.

To this end, we analysed each set of unloading and subsequent loading curves for our stress-cycle experiments (Fig. 3a) and adequately fitted both curves with third-order polynomial relationship in order to capture the true form of the stress–strain curve with two inflexion points. These

Table 1
Experimental conditions. UCS-unconfined compression strength, DNF-did not fail

Sample	Experiment type	Cycle amplitude	Cycles to failure	Load-hold stress	Load-hold time (hrs)	Number of hold periods	Failure stress (MPa)	Notes
WG-1	UCS	N/A	1	N/A	N/A	N/A	190	
WG-2	UCS	N/A	1	N/A	N/A	N/A	205	
WG-3	Increasing amplitude	Small	10	N/A	N/A	N/A	195	Cycle amplitude too small in WG-03 and 04
WG-4	Increasing amplitude	Small	10	N/A	N/A	N/A	193	
WG-5	Increasing amplitude	Large	0	N/A	N/A	N/A	133	Test failed
WG-6	Increasing amplitude	Large	7	N/A	N/A	N/A	169	
WG-7	Constant amplitude	N/A	N/A	0.7UCS	1	0	DNF	Test failed
WG-8	Increasing amplitude	Large	0	N/A	N/A	N/A	196	
WG-9	Constant amplitude	N/A	N/A	0.7UCS	1	6	DNF	
WG-10	Constant amplitude	N/A	N/A	0.8UCS	1	6	DNF	
WG-11	Constant amplitude	N/A	N/A	0.8UCS	0.5	6	DNF	
WG-12	Constant amplitude	N/A	N/A	0.8UCS	0.75	6	DNF	
WG-13	Constant amplitude	N/A	N/A	0.8UCS	6	6	DNF	

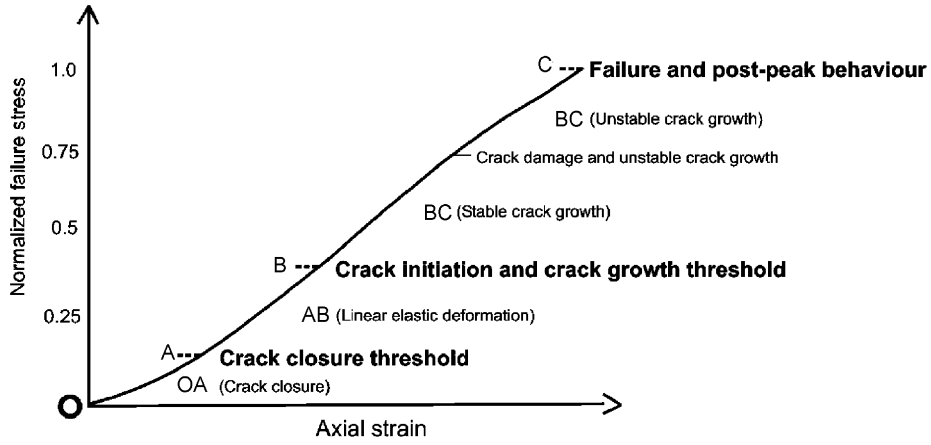

Fig. 2. Schematic diagram showing the general shape of the stress–strain curve in a typical experiment. Also shown are the approximate positions of the stages of crack development in brittle rock under uniaxial compression [55–57].

fits can be differentiated so that tangent modulus can be calculated for any given stress. The tangent modulus was calculated for both of the curves at 10 MPa and then at every 10 MPa increment thereafter. Perfect elasticity has been assumed where the gradients of unloading and the subsequent loading curves are approximately equal (Fig. 3b) despite the hysteresis. We contend that by comparing an unloading curve with a subsequent loading curve, no additional microcrack damage will be imparted to the specimen until the previous highest stress on the loading cycle is exceeded. This assertion is supported by acoustic emission analysis made in triaxial tests conducted by other workers during stress cycling and is termed the Kaiser effect (see reviews by Holcomb [58], Lockner [59] and Lavrov [60]). However, in our experiments AE events were not recorded; in some stress-cycling studies AE have been recorded [52,61,62]. If the gradients are equal, we assume that the same micromechanical processes are operating both during unloading and subsequent loading. Hence, although hysteresis maybe present, if the same tangent modulus is reproducible during both unloading and loading, we have assumed these values provide a reasonable approximation of the perfect elastic properties (and are hence termed 'Young's modulus' in our reported

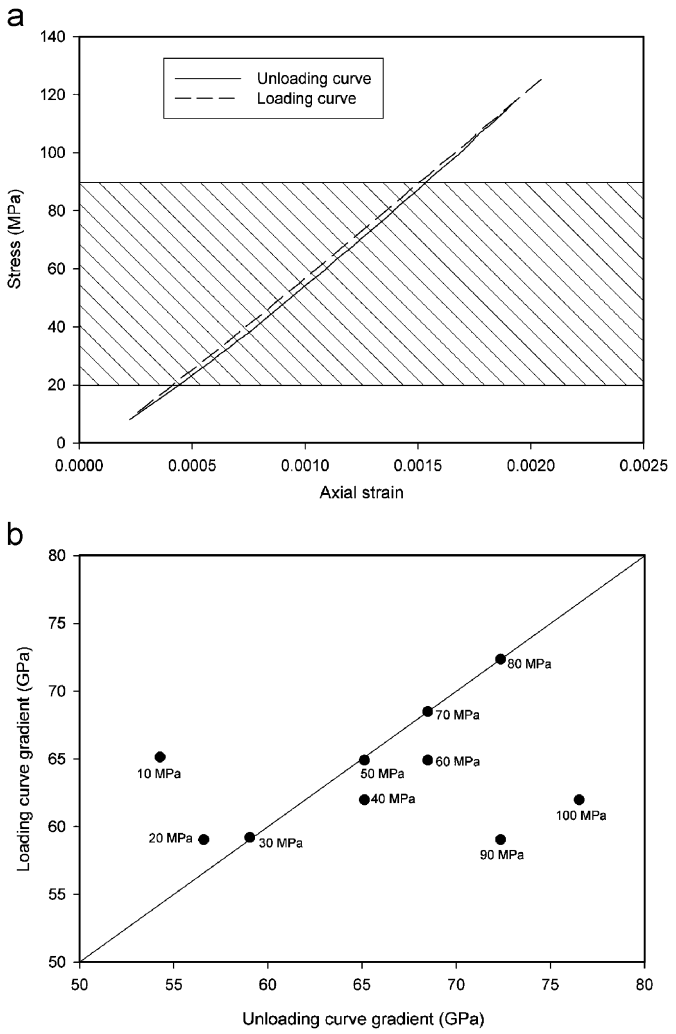

Fig. 3. (a) Example of one of the sets of unloading and subsequent loading curves taken from sample WG-08. Hatched area denotes area where elasticity has been confirmed using the approach detailed in the text. Outside of the hatched area, the data were not used to determine elastic properties. (b) Plot showing the calculated unloading and subsequent loading curve gradients (Young's moduli) for the set of curves in (a). Values were excluded from the dataset if they deviated by more than 5 GPa from the line of equal gradient (in this case 10, 90 and 100 MPa).

data). Our data, obtained in this way, show that the Poisson's ratio does not extend above 0.5 and as such suggests the validity of our approach. This method has allowed us to greatly extend the region in which the elastic properties can be obtained.

3. Experimental results

3.1. Increasing-amplitude cyclic experiments

In order to try to investigate the evolution of static elastic properties as rock approaches failure samples of Westerly granite were subjected to increasing-amplitude cyclic loading experiments. The stress-peak of the large-amplitude cycles started at ~80 MPa (~0.4UCS) and was increased by ~12 MPa after each completed cycle until the sample failed. The low starting value ensured that an acceptable number of cycles were completed before rock failure and so that the changes in static elastic properties as the sample approached failure could be recorded in detail. Fig. 4 shows a representative stress–strain curve during increasing-amplitude cyclic loading for Westerly granite (sample WG-08). The graph shows that permanent strain has accumulated during experimentation and therefore crack damage mechanisms must have been operative. The approximate locations of the stages of stress–strain behaviour for brittle material [55–57] are indicated (as in Fig. 2). Their positions are termed 'approximate' since Eberhardt et al. [63] found that they are more accurately determined using an approach that combines AE event counts with a moving point regression analysis. Brace et al. [56] defined the position of crack initiation (stage B) to be 0.3–0.5 UCS and Bieniawski [57] suggested that unstable crack growth is likely to occur between 0.7–0.85 UCS. The boundary between the crack closure threshold stage (stage A) and the linear elastic deformation region (region AB) was simply defined by the change to a linear gradient (Fig. 2).

From these data, and using our test for 'perfect' elasticity, the Young's modulus and Poisson's ratio were calculated (from sample WG-08) and their evolution plotted with respect to stress (Fig. 5a) and number of cycles (Fig. 5b). Both graphs demonstrate that large-amplitude stress cycling results in an overall reduction in sample stiffness. Fig. 5a shows that elastic properties exhibit a strong stress-dependency. If a single stress cycle is considered in Fig. 5a (cycle 7 in this example), Young's modulus is seen to increase rapidly (total increase of ~46% from 20 to 100 MPa), whereas Poisson's ratio demonstrates only a very modest decrease with respect to increasing stress, until the last few cycles when a larger decrease is observed. Both elastic properties are seen to change at relatively constant rates. If a single stress value is considered in Fig. 5b (50 MPa in this example), the Young's modulus is seen to decrease (~11%) and the Poisson's ratio increase (~43%) as the number of cycles is increased and before the sample reaches failure. Young's modulus is seen to decrease at a relatively constant rate; however, Poisson's ratio is seen to increase exponentially just before failure. It must be noted that number of cycles is not an independent variable since their amplitude increased with each successive cycle. Mechanisms operating during the increasing-amplitude experiments have large effect on the evolution of static elastic properties.

3.2. Constant-amplitude cyclic experiments

Samples of Westerly granite were also subjected to constant-amplitude cyclic experiments. In such experiments, time-dependent effects such as stress corrosion were encouraged by implementing 'load-hold' periods between cycles so that its influence on static elastic properties could be investigated. Cycles were required to evaluate the effect

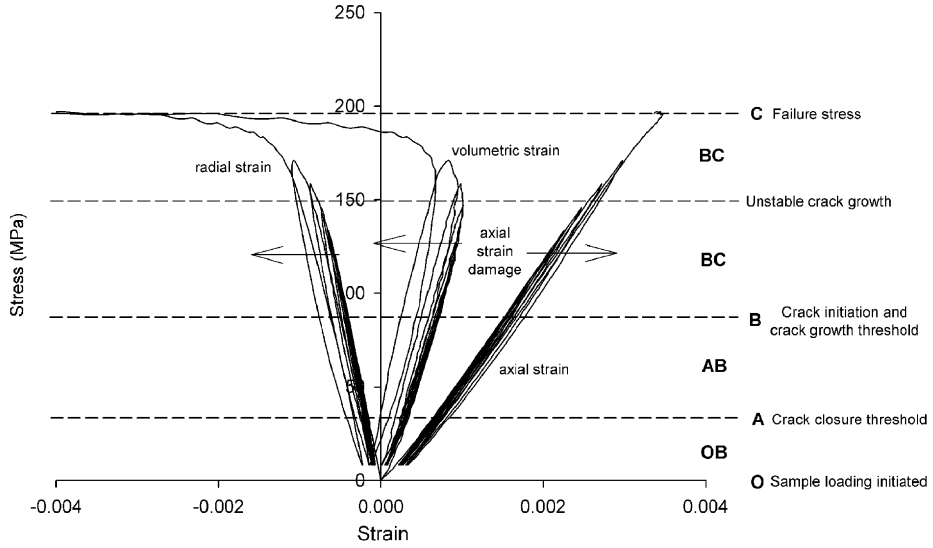

Fig. 4. Representative stress–strain curve for Westerly granite under increasing-amplitude cyclic loading (sample WG-08). Stress–strain stages have also been included as in Fig. 2 [55–57]. Arrows indicate how the axial, circumferential and volumetric strains change during the accumulation of microcrack damage during the experiment.

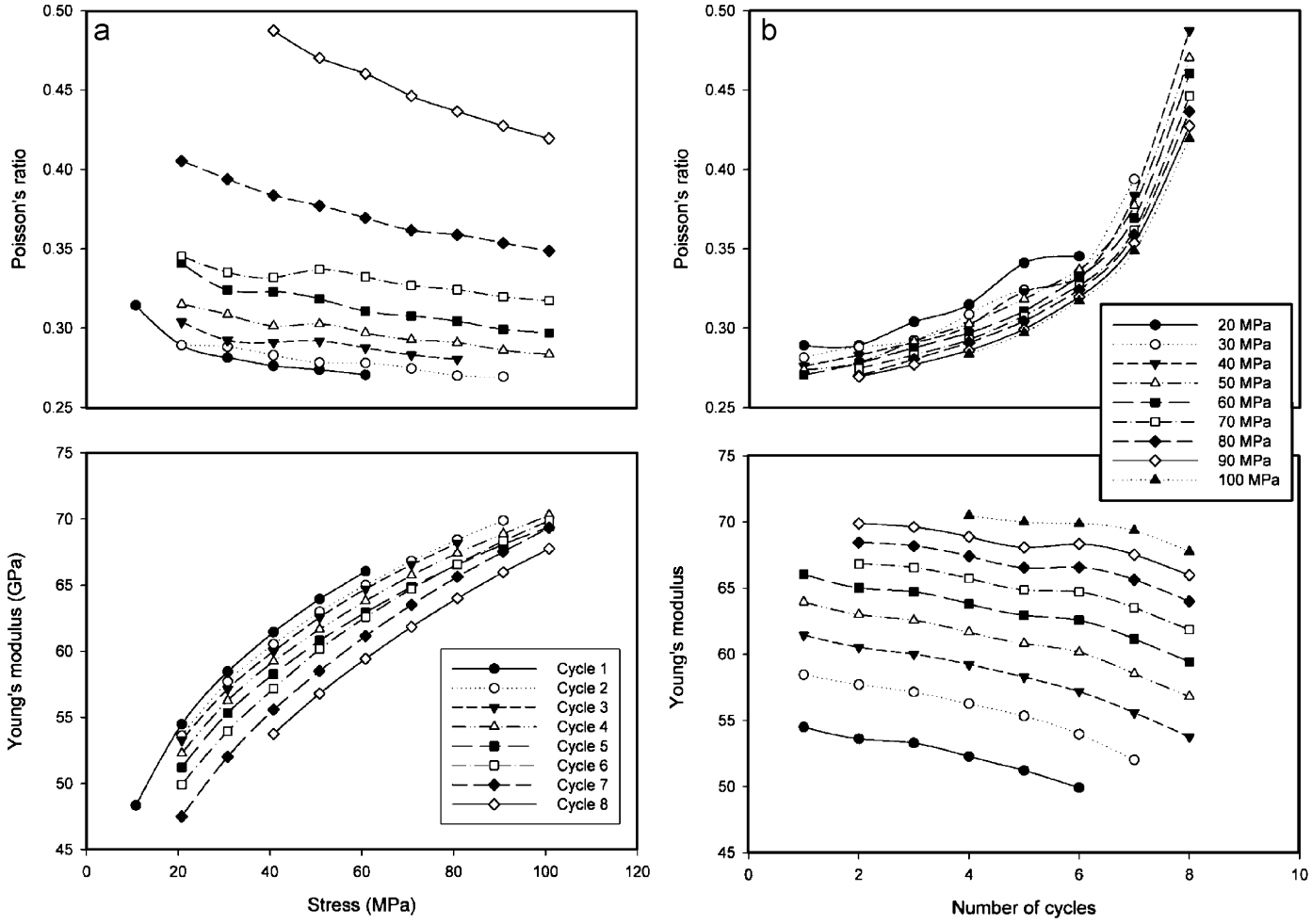

Fig. 5. (a) Elastic property development in Westerly granite with increasing stress during increasing-amplitude cyclic experiments (sample WG-08). (b) Elastic property development in Westerly granite with increasing number of cycles during increasing-amplitude cyclic experiments (sample WG-08).

of stress corrosion on static elastic property development since stress–strain curves are necessary for their calculation. The experiments were performed at two different proportions of the unconfined compressive strength (%UCS) and load-hold durations between cycles were also varied between experiments (see Table 1 for test conditions). Experiments were carried out at load-hold axial stresses of either 0.7 UCS or 0.8 UCS—both within the unstable crack propagation region as defined by Bieniawski [57]. High stresses at the load-hold periods were selected in an attempt to ensure the effect of stress corrosion can be seen within laboratory timescales. The UCS was assumed using the average failure stress from two conventional UCS tests (samples WG-01 and WG-02). We note that as crack damage accumulates in the sample during experimentation then the UCS will decrease, therefore the %UCS used in the hold periods is expected to have increased slightly during testing. Fig. 6 shows a representative stress–strain curve for Westerly granite during a constant-amplitude experiment (sample WG-10). The graph shows that only a small amount of permanent strain accumulated during experimentation and therefore crack damage mechanisms must have been operating, albeit at a lesser extent compared to increasing-amplitude experiments.

Using the methodology outlined previously, the evolution of the elastic properties has been calculated with respect to number of cycles for sample WG-10 (Fig. 7). It shows that crack damage mechanisms cause a gradual reduction in sample stiffness with respect to number of cycles, equating to a small decrease in Young's modulus (~1%) and a more substantial increase in Poisson's ratio (~13%). Both are seen to change at a relatively constant rate with respect to number of cycles. Decreasing the %UCS from 0.8 to 0.7 UCS the percentage decrease in Young's modulus remains approximately the same; however, the increase in Poisson's ratio reduces to ~6%. However, the data from just the load-hold periods show

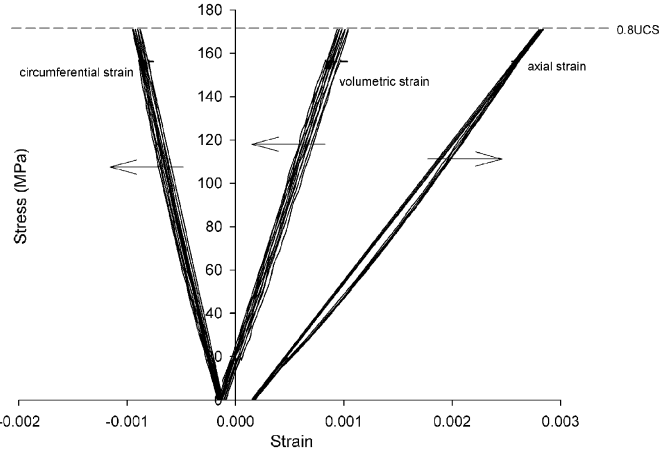

Fig. 6. Typical stress–strain curve for Westerly granite under constant-amplitude cyclic loading (sample WG-10). Arrows indicate how the axial, circumferential and volumetric strains change during the accumulation of microcrack damage during the experiment.

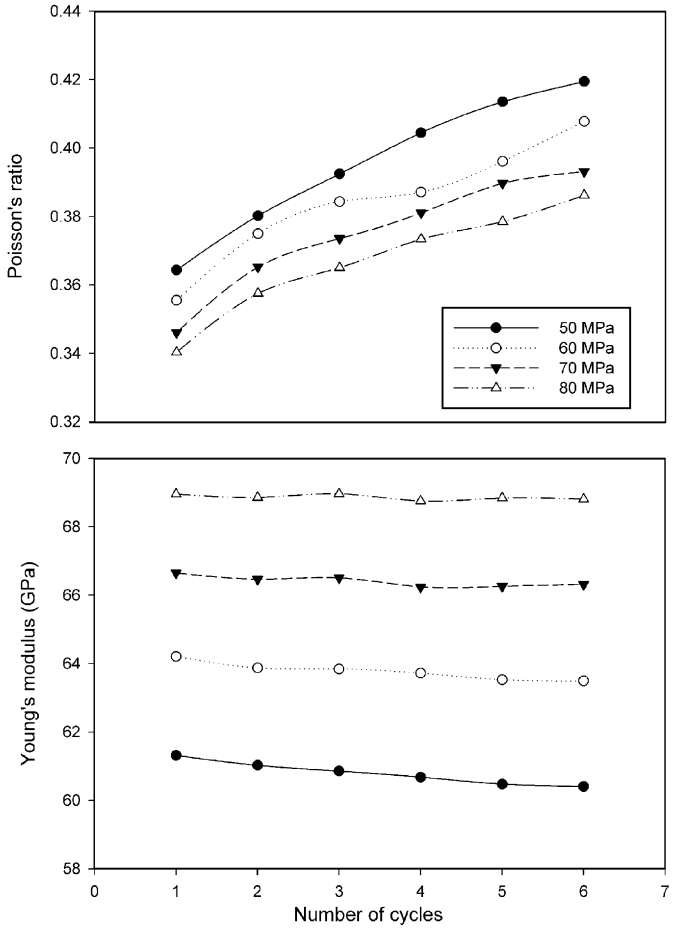

Fig. 7. Elastic property development in Westerly granite with increasing number of cycles during a constant-amplitude cyclic experiment (sample WG-10).

that time-dependent effects are almost negligible to the development of static elastic properties over the timeframe and conditions under which the experiments were conducted. The axial strain values showed no variation, within error, over any of the load-hold periods and immediately proceeding stress cycles there are obvious 'jumps' in axial strain. Therefore, the accumulated damage seen in Fig. 7 is likely to be largely the result of large-amplitude stress cycling. Sample WG-13 validated this hypothesis and showed that, without cycles, little variation in axial strain damage is observed over the implemented experimental timeframe and conditions. Mechanisms operating during the constant-amplitude experiments have an overall modest effect on the evolution of static elastic properties.

4. Discussion

Experimental rock mechanics has defined three types of microcracking. (1) Stress-induced microcracking, where the stress locally exceeds a fracture criterion, causing the crack to propagate spontaneously. Crack propagation is either stable or unstable. (2) Cyclic fatigue microcracking, where cracking is produced by the working of cracks as they open

and close in response to cyclic loading. (3) Time-dependent microcracking, where stable crack growth occurs below the critical stress intensity factor (Kc), and are due to several competing factors of which the most familiar is stress corrosion [23,24,26,64,65]. Rock fracture is sensitive to which type is prevalent and mechanisms act simultaneously and independently [66].

In our experiments it is difficult or impossible to distinguish between the three mechanisms of microcrack growth. However we can say that the contribution of time-dependent crack growth is almost negligible to the development of static elastic properties under the implemented experimental timeframe and conditions for Westerly granite. Stress corrosion leading to time-dependent creep is undoubtedly taking place, but at an insufficient rate and magnitude required to observe its effect on the static elastic properties. A possible explanation for this is that the use of strain gauges restricted our experiments to dry conditions only. Most experiments designed to promote and observe time-dependent brittle creep are conducted under water-saturated conditions. Also, Westerly granite is a fine-grained, crystalline rock with a low porosity and low initial crack density and thus inhibits the transport of reactive species to the crack tips. Despite using significantly increased hold times than used in experiments by Lau and Chandler [17], we conclude the hold times need to be longer to observe the effect of time-dependent microcracking under our experimental conditions.

We attribute the gradual degradation in sample stiffness with respect to number of increasing amplitude stress cycles (Fig. 5b) to the growth and coalescence of pre-existing and newly initiated microcracks. This is corroborated by thin section analysis. After eight large-amplitude stress cycles the rock is seen to contain many more microcracks (Fig. 8b) when compared with an undeformed sample (Fig. 8a). The microcracks are predominantly large intragranular and transgranular microcracks and display a preferred axial orientation (Figs. 8c and d). Fig. 5b shows that the Poisson's ratio increases exponentially just before failure (the last few cycles). As microcrack damage accumulates within the sample, predominantly in an axial crack orientation, then the circumferential strain increase becomes more prevalent relative to the decreasing axial strain. Hence the Poisson's ratio increases as crack damage is accumulated in the sample. The most plausible explanation for the stress-dependency of the Young's modulus shown in Fig. 5a is that the stress acts to close oblique and transversely orientated microcracks with increasing axial load; this can be related to the mean stress increase during loading. However, it must be noted that Westerly granite has a low initial crack density and Fig. 8 only shows a modest number of oblique and transversely orientated microcracks.

Our experimental data were collected under uniaxial conditions and the elastic property evolution may differ under a confining pressure [67]. Indeed, experiments have shown that the onset of dilatancy in Westerly granite is reduced by cyclic loading under uniaxial conditions but remain largely unaffected under triaxial conditions [68]. This implies that, under triaxial conditions, the effect of

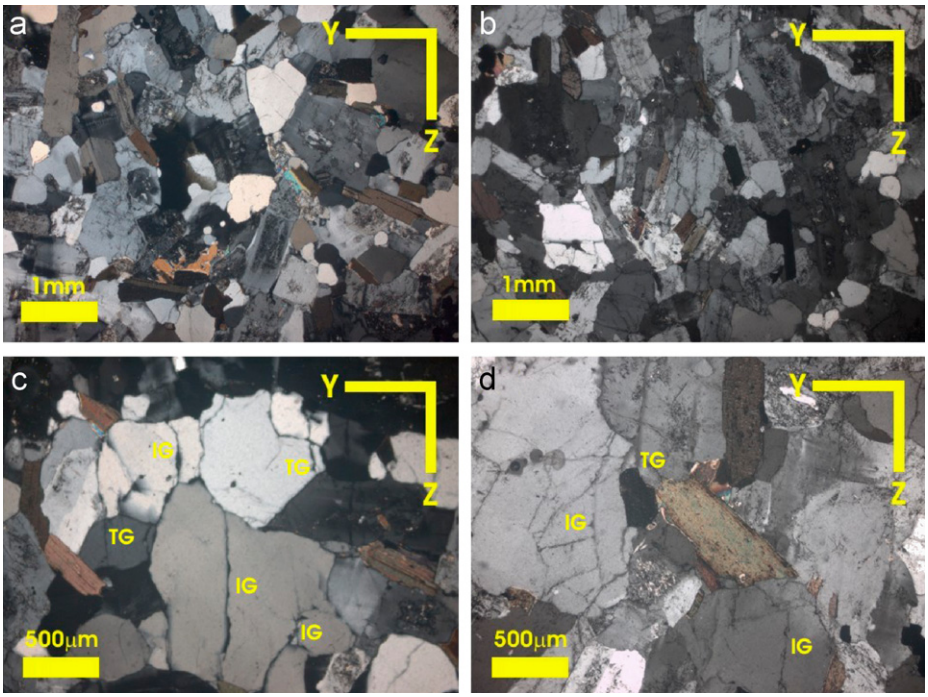

Fig. 8. Photomicrographs of Westerly granite under cross-polarized light. (a) undeformed sample. (b) Sample WG-08 after eight large-amplitude stress cycles. (c) and (d) Magnified photomicrographs of sample WG-08 after eight large-amplitude stress cycles showing large intragranular and transgranular microcracks in grains of quartz. Thin sections were taken along the *YZ* plane (see Fig. 1 for sample orientation) and axial compression was in the *Z*-direction. IG—intragranular microcrack; TG—transgranular microcrack.

stress-cycling on elastic moduli would be reduced. There are very few experimental studies of the evolution of rock elasticity prior to failure under a confining pressure. However, some dynamic elastic properties calculated from seismic velocity measurements from tests taken to failure at confining pressure are available for comparison. Ayling et al. [20] monitored dynamic elastic property changes in Darley Dale sandstone deformed at 50 MPa confining pressure. Although a different rock type was used in this experiment the changes seen in our results are of the same magnitude.

In nature, in addition to the microscopic damage imparted to our experimental samples, meso- and macro-scale fractures present within the Earth's crust will further reduce the overall bulk elastic properties of a rock mass. The effect of these larger scale features on elastic moduli is impossible to determine at the laboratory scale. Hence our data may be viewed as a 'minimum' effect that might be observed as it does not account for this additional effect. Finally, our data relate only to low porosity crystalline rocks whereas in nature deformation affects a wide variety of rock types that may possess different porosities, elastic properties or a mechanical anisotropy. However, such data are invaluable for an insight into the magnitude of static elastic property evolution with deformation and trends between the variables; and crystalline rock is commonly fractured at depth.

5. Conclusions

We have presented a new methodology to help identify perfect elasticity in stress–strain experiments. Previously, reliable data has only been obtained from the linear elastic portion of the stress strain curve. Our methodology enhances the range of stress values from which the elastic properties can be calculated and allows a detailed study into the evolution of the static elastic properties of rock as it approaches failure.

Our data show that significant changes in the static elastic properties occur as crystalline rock accumulates microcrack damage. If the elastic properties are monitored for a constant stress but as a function of number of increasing amplitude stress cycles, the changes seen equate to a decrease in Young's modulus of ~11% and a substantial increase in Poisson's ratio (~43%) before the rock reaches failure (Fig. 5b).

Our data indicate a strong stress-dependency of static Young's modulus (~46% increase) within a single loading cycle (Fig. 5a). At low loads there is an increase in Young's modulus in the region OA due to crack closure. The elastic properties stay constant in the linear elastic region AB. Above B there is an increase in Young's modulus until the behaviour becomes inelastic by exceeding the previous highest applied stress.

We were not able to distinguish between different modes of crack initiation and growth, such as stress induced microcracking or cyclic fatigue microcracking. However, we are able to say that under the dry test conditions and timescales used in experiments, time-dependent microcracking plays a very minor role in the development of the elastic properties.

Acknowledgements

M.H. gratefully thanks the Nuffield Foundation Undergraduate Research Bursary for financial support; Dave Prior, D. Healy and Phil Meredith for helpful comments and suggestions; and Tom Mitchell and Peter Armitage for help and support during the experimentation. The authors also thank Brian Evans for providing the Westerly granite block, and our reviewers for their helpful comments and suggestions on improvements to the manuscript.

References

[1] Griffith AA. The phenomenon of rupture and flow in solids. Trans Royal Soc Phil Series A 1920;221:163–98.
[2] Griffith AA. The theory of rupture. In: Biezeno CB, Burgers JM, editors. Proc Int Cong Appl Mech. Delft: Tech Boekhandel en Drukkerij J Walter Jr; 1924. p. 54–63.
[3] Brace WF, Bombolakis EG. A note on brittle crack growth in compression. J Geophys Res 1963;68:3709–13.
[4] Scholz CH. Microfracturing and the inelastic deformation of rock in compression. J Geophys Res 1968;73:1417–32.
[5] Peng S, Johnson AM. Crack growth and faulting in cylindrical specimens of Chelmsford granite. Int J Rock Mech Min Sci 1972;9:37–86.
[6] Anders MH, Wiltschko DV. Microfracturing, paleostress and the growth of faults. J Struct Geol 1994;16:795–815.
[7] Moore DE, Lockner DA. The role of microcracking in shear-fracture propagation in granite. J Struct Geol 1995;17:95–114.
[8] Vermilye JM, Scholz CH. The process zone: A microstructural view of fault growth. J Geophys Res 1998;103:12223–37.
[9] Janssen C, Wagner FC, Zang A, Dresen G. Fracture process zone in granite: a microstructural analysis. Int J Earth Sci (Geol Rundsch) 2001;90:46–59.
[10] Wilson JE, Chester JS, Chester FM. Microfracture analysis of fault growth and wear processes, Punchbowl Fault, San Andreas system, California. J Struct Geol 2003;25:1855–73.
[11] Faulkner DR, Mitchell TM, Healy D, Heap MJ. Slip on 'weak' faults by the rotation of regional stress in the fracture damage zone. Nature 2006;444:922–5.
[12] Scholz CH. The mechanics of earthquakes and faulting. Cambridge: Cambridge University Press; 2002.
[13] Gudmundsson A. Effects of Young's modulus on fault displacement. Compt Rend Geosci 2004;336:85–92.
[14] Peltzer G, Crampé F, King G. Evidence of nonlinear elasticity of the crust from the Mw 7.6 Manyi (Tibet) earthquake. Science 1999;286:272–6.
[15] Barenblatt GI. The mathematical theory of equilibrium cracks in brittle fracture. Adv App Mech 1962;7:55–80.
[16] Brown ET, Bray JW, Santarelli FJ. Influence of stress-dependent elastic moduli on stresses and strains around axisymmetric boreholes. Rock Mech Rock Eng 1989;22:189–203.
[17] Lau JSO, Chandler NA. Innovative laboratory testing. Int J Rock Mech Min Sci 2004;41:1427–45.
[18] Alm O, Jaktlund L, Shaoquan K. The influence of microcrack density on the elastic and fracture mechanical properties of Stripa granite. Phys Earth Planet Inter 1985;40:161–79.
[19] Martin CD, Chandler NA. The progressive fracture of Lac du Bonnet granite. Int J Rock Mech Min Sci 1994;31:643–59.
[20] Ayling MR, Meredith PG, Murrell SAF. Microcracking during triaxial deformation of porous rocks monitored by changes in rock

physical properties, I. Elastic-wave propagation measurements on dry rocks. Tectonophys 1994;245:205–21.
[21] Eberhardt E, Stead D, Stimpson B. Quantifying progressive pre-peak brittle fracture damage in rock during uniaxial compression. Int J Rock Mech Min Sci 1999;36:361–80.
[22] Lyakhovsky V, Reches Z, Weinberger R, Scott TE. Non-linear elastic behaviour of damaged rocks. Geophys J Int 1997;130:157–66.
[23] Atkinson BK. Subcritical crack propagation in rocks: Theory, experimental results and applications. J Struct Geol 1982;4:41–56.
[24] Atkinson BK. Subcritical crack-growth in geological materials. J Geophys Res 1984;89:4077–114.
[25] Schmidtke RH, Lajtai EZ. The long-term strength of Lac du Bonnet granite. Int J Rock Mech Min Sci 1985;22:461–5.
[26] Atkinson BK, Meredith PG. Experimental fracture mechanics data for rocks and minerals. In: Atkinson BK, editor. Fracture mechanics of rock. London: Academic Press; 1987. p. 477–525.
[27] Lockner DA. A generalised law for brittle deformation of Westerly granite. J Geophys Res 1998;103:5107–23.
[28] Katz O, Reches Z. Pre-failure damage, time-dependent creep and strength variations of a brittle granite. In: Proc fifth International conference on anal discontinuous deformation. Ben-Gurion University. Rotterdam: Balkema; 2002.
[29] Birch F. The velocity of compressional waves in rocks to 10 kilobars, 1. J Geophys Res 1960;65:1083–102.
[30] Birch F. The velocity of compressional waves in rocks to 10 kilobars, 2. J Geophys Res 1961;66:2199–224.
[31] Walsh JB. The effect of cracks on the compressibility of rock. J Geophys Res 1965;70:381–9.
[32] Anderson DL, Minster B, Cole D. The effect of orientated cracks on seismic velocities. J Geophys Res 1974;79:4011–5.
[33] O'Connell RJ, Budiansky B. Seismic velocities in dry and saturated cracked solids. J Geophys Res 1974;79:5412–26.
[34] Soga N, Mizutani H, Spetzler H, Martin RJI. The effect of dilatancy on velocity anisotropy in Westerly granite. J Geophys Res 1978;83:4451–8.
[35] Sayers CM, Kachanov M. Microcrack induced elastic wave anisotropy in brittle rocks. J Geophys Res 1995;100:4149–56.
[36] Guéguen Y, Schubnel A. Elastic wave velocities and permeability of cracked rocks. Tectonophys 2003;370:163–76.
[37] Reuschlé T, Gbaguidi Haore S, Darot M. Microstructural control on the elastic properties of thermally cracked granite. Tectonophys 2003;370:95–104.
[38] Fortin J, Schubnel A, Guéguen Y. Elastic wave velocities and permeability evolution during compaction of Bleurswiller sandstone. Int J Rock Mech Min Sci 2005;42:873–89.
[39] Takemura T, Oda M. Changes in crack density and wave velocity in association with crack growth in triaxial tests of Inada granite. J Geophys Res 2005;110:B05401, doi:10.1029/2004JB003395.
[40] Simmons G, Brace WF. Comparison of static and dynamic measurements of compressibility of rocks. J Geophys Res 1965;70:5649–56.
[41] Cheng CH, Johnston DH. Dynamic and static moduli. Geophys Res Lett 1981;8:39–42.
[42] Eissa EA, Kazi A. Relation between static and dynamic Young's moduli of rocks. Int J Rock Mech Min Sci Geomech Abstr 1989;25:479–82.
[43] Ciccotti M, Mulargia F. Differences between static and dynamic elastic moduli of a typical seismogenic rock. Geophys J Int 2004;157:474–7.
[44] Ciccotti M, Almagro R, Mulargia F. Static and dynamic moduli of the seismogenic layer in Italy. Rock Mech Rock Eng 2004; doi:10.1007/s00603-003-0019-7.
[45] Glover PWJ, Baud P, Darot M, Meredith PG, Boon SA, LeRevelec M, Zoussi S, Reuschle T. α/β phase transition in quartz monitored using acoustic emissions. Geophys J Int 1995;120:775–82.
[46] Haimson BC, Chang C. A new true triaxial cell for testing mechanical properties of rock, and its use to determine rock strength and deformability of Westerly granite. Int J Rock Mech Min Sci 2000;37:285–96.
[47] Hadley K. Azimuthal variation of dilatancy. J Geophys Res 1975;80:4835–50.
[48] Hadley K. The effect of cyclic stress on dilatancy, another look. J Geophys Res 1976;81:2471–4.
[49] Scholz CH, Koczynski TA. Dilatancy anisotropy and the response of rock to large cyclic loads. J Geophys Res 1979;84:5525–34.
[50] Engelder T. Stress regimes in the lithosphere. Princeton: Princeton University Press; 1993.
[51] Takemura T, Golshani A, Oda M, Suzuki K. Preferred orientations of open microcracks in granite and their relation with anisotropic elasticity. Int J Rock Mech Min Sci 2003;40:443–54.
[52] Sondergeld CH, Estey LH. Acoustic emission study of microfracturing during the cyclic loading of Westerly granite. J Geophys Res 1981;86:2915–24.
[53] Hawkes I, Mellor M. Uniaxial testing in rock mechanics laboratories. Eng Geol 1970;4:177–285.
[54] Paterson MS, Wong T-F. Experimental Rock Deformation: The Brittle Field. Berlin: Springer; 2005.
[55] Jaeger JC, Cook NGW, Zimmerman RW. Fundamentals of rock mechanics. 4th ed. Oxford: Blackwell; 2007.
[56] Brace WF, Paulding B, Scholz CH. Dilatancy in the fracture of crystalline rocks. J Geophys Res 1966;71:3939–53.
[57] Bieniawski ZT. Mechanism of brittle rock fracture, parts I, II and III. Int J Rock Mech Min Sci Geomech Abstr 1967;4:395–430.
[58] Holcomb D. General theory of the Kaiser effect. J Rock Mech Min Sci Geomech Abstr 1993;30:929–35.
[59] Lockner D. The role of acoustic emission in the study of rock fracture. Int J Rock Mech Min Sci Geomech Abstr 1993;30:883–99.
[60] Lavrov A. The Kaiser effect in rocks: principals and stress estimation techniques. Int J Rock Mech Min Sci 2003;40:151–71.
[61] Rao MVMS, Ramana YV. A study of progressive failure of rock under cyclic loading by ultrasonic and AE monitoring techniques. Rock Mech Rock Eng 1992;25:237–51.
[62] Stanchits S, Vinciguerra S, Dresen G. Ultrasonic velocities, acoustic emission characteristics and crack damage of basalt and granite. Pure Appl Geophys 2006;163:974–93.
[63] Eberhardt E, Stead D, Stimpson B, Read RS. Identifying crack initiation and propagation thresholds in brittle rock. Can Geotech J 1998;35(2):222–33.
[64] Anderson OL, Grew PC. Stress corrosion theory of crack propagation with applications to geophysics. Rev Geophys Space Phys 1977;15:77–104.
[65] Costin LS. Time-dependent deformation and failure. In: Atkinson BK, editor. Fracture Mechanics of Rock. London: Academic Press; 1987. p. 167–215.
[66] Costin LS, Holcomb DJ. Time-dependent failure of rock under cyclic loading. Tectonophysics 1981;79:279–96.
[67] Christensen NI, Wang HF. The influence of pore pressure and confining pressure on dynamic elastic properties of Berea sandstone. Geophysics 1985;50:207–13.
[68] Zoback MD, Byerlee JD. The effect of cyclic differential stress on dilatancy in Westerly granite under uniaxial and triaxial conditions. J Geophys Res 1975;80:1526–30.